Nuclear structure of odd-odd ^{82}Y

P. C. Womble, J. Döring, T. Glasmacher,* J. W. Holcomb, G. D. Johns, T. D. Johnson, T. J. Petters, M. A. Riley, V. A. Wood, and S. L. Tabor
Department of Physics, Florida State University, Tallahassee, Florida 32306

P. Semmes
Department of Physics, Tennessee Technological University, Cookeville, Tennessee 38505
(Received 23 February 1993)

Excited states in ^{82}Y have been investigated via the ^{58}Ni(^{28}Si,3pn)^{82}Y and ^{56}Fe(^{29}Si,$p2n$)^{82}Y reactions using beams provided by the Florida State University Tandem-LINAC with energies of 95 to 135 MeV. Particle-γ coincidences with a full-sphere charged-particle detector and an excitation curve were used to assign γ rays to ^{82}Y. The ^{56}Fe(^{29}Si,$p2n$)^{82}Y reaction at 95 MeV was used to measure γ-γ coincidences with five Compton-suppressed Ge detectors. Lifetimes in the ns and ps ranges were measured using direct timing and the Doppler-shift attenuation method. A level scheme with 39 states was constructed up to tentative spins and parities of (15^-) and (21^+). In the positive-parity yrast band a phase reversal was observed in the signature splitting at $I = 10\hbar$. The $B(M1)$ strengths in this band alternate with signature between about 0.1 and 1.0 μ_N^2. The $B(E2)$ strengths of about 90 Weisskopf units are in good agreement with those predicted by Hartree-Fock-Bogolyubov calculations. Particle-rotor calculations indicate a prolate or triaxial core shape for the positive-parity band.

PACS number(s): 21.10.−k, 23.20.−g, 27.50.+e

I. INTRODUCTION

Nuclei in the $A \approx 80$ region show a rich variety of structural behavior at high angular momenta. These effects have been attributed with a high degree of success to the interplay between the Coriolis force, deformation, and pairing. The shapes of nuclei in this region are soft to the polarizing effects of rotation and quasiparticle (qp) alignment. The same unique parity $g_{9/2}$ orbital plays the dominant role in high-spin phenomena for both neutron and proton quasiparticles.

Odd-odd nuclei have not been studied as extensively as their neighbors, but recent investigations of nearby odd-odd isotopes, such as ^{74}Br[1], ^{76}Br[2], and ^{80}Rb[3] have shown a similar well developed rotational structure starting above 0.5 MeV excitation energy. Although the pairing of like particles is an important aspect of nuclear structure at low excitation energy and qp alignment has major effects on the behavior of rotational bands, much less is known about the residual proton-neutron interaction. The reversal of signature splitting which has been observed at about a spin of $9\hbar$ in many odd-odd nuclei was predicted [4] to result from the competition between qp coupling and collective rotation. The exact spin at which it occurs may depend on the p-n residual interaction. An alternating pattern in the $B(M1)$ strengths within a band has been reported for all types of nuclei in the $A \approx 80$ region, but seems most prevalent in the odd-odd ones. The effect has been attributed [5, 6] to triaxiality in 1-qp bands, but its behavior in 2-qp bands needs further investigation.

Prior to the present investigation experimental information on the odd-odd nucleus ^{82}Y was very limited. A half-life of 9.5 s had been measured [7, 8] for the ground state, and a spin and parity of 1^+ had been assigned [7, 9] to the ground state based on allowed β decays to the lowest 0^+ and 2^+ states in ^{82}Sr. A preliminary level scheme had been produced [10] from an earlier γ-γ coincidence experiment. As this manuscript was being prepared we learned of a preliminary report [11] on a new investigation of high-spin states in ^{82}Y.

The present work involves the identification of transitions in ^{82}Y, the determination of the level scheme from prompt γ-γ coincidences and directional correlation ratios, and measurements of lifetimes in the ns and ps ranges using direct timing and the Doppler-shift attenuation method. The observed band structures are compared with those of neighboring $N = 43$ isotones and $Z = 39$ isotopes and are discussed within the framework of the cranking and particle-rotor models.

II. EXPERIMENTAL METHODS

Four experiments were performed to measure the properties of excited states in ^{82}Y. To identify the γ rays associated with ^{82}Y, an experimental excitation curve was measured and compared with the results predicted by statistical model calculations. Also, p-γ coincidences were measured with a phoswich charged-particle detector array to identify the reaction channel associated with these γ rays. A prompt γ-γ coincidence experiment was performed to determine the level scheme of ^{82}Y, directional correlation ratios, and ps lifetimes of high-spin

*Present address: National Superconducting Cyclotron Laboratory, Michigan State University, East Lansing, MI 48824-1321.

states via the Doppler-shift attenuation method. Finally, a delayed coincidence measurement was carried out to determine ns lifetimes for isomers in the low-spin region.

A. Identification of ^{82}Y

The fusion evaporation reaction ^{58}Ni(^{28}Si,3pn)^{82}Y was used to obtain experimental cross sections for the excitation curve. A beam of ^{28}Si was accelerated to energies of 95 to 135 MeV in 10 MeV increments by the Florida State University Tandem-LINAC facility. The target was natural Ni of which ^{58}Ni is 68% abundant. The target had a thickness of about 500 μg/cm^2. A single bismuth germanate (BGO) Compton-suppressed high purity Ge (HPGe) detector was placed perpendicular to the beam axis to detect γ rays from the reaction. The computer code PACE2 (projected angular-momentum coupled evaporation) [12] was used to calculate the cross sections for the ^{28}Si + ^{58}Ni reaction.

Experimental cross sections were determined by addition of the intensities of ground state transitions multiplied by a normalization factor. To determine this factor, as many reaction products as possible were identified. Their experimental cross sections were determined, summed (excluding ^{82}Y) and then normalized to the same percentage yield as PACE2 predicted for the sum of the same nuclei. These sums accounted for most of the predicted total reaction yield. In cases where the ground state transitions were obscured, other lines in the same nucleus were used.

Figure 1 shows a graph of experimental yields versus laboratory energy, and PACE2 predictions for various nuclei produced in the ^{28}Si + ^{58}Ni reaction. The intensities of the lines attributed to ^{82}Y follow the trends predicted for that nucleus quite well and differ substantially from the predictions for ^{81}Y and ^{83}Y. The curves for ^{82}Y (3pn evaporation) and ^{82}Sr (4p) are quite similar but the transitions in ^{82}Sr are well known, and no coincidences have been seen between the suggested ^{82}Y lines and the many known ones in ^{82}Sr. The fact that these lines occur in both the ^{58}Ni(^{28}Si,3pn) and ^{56}Fe(^{29}Si,$p2n$) reactions in which ^{82}Y is predicted to be one of the dominant products lends weight to the argument that these lines belong to ^{82}Y. The existence of several ns isomers, as discussed below, provides further evidence that these γ-decay sequences occur in an odd-odd nucleus.

Charged-particle-γ coincidence measurements were also used to provide an elemental identification for the γ-decay sequence. The ^{56}Fe(^{29}Si,$p2n$) reaction was used for this experiment. The ^{29}Si ions were obtained from the 4.67% abundance in a natural Si sample in the Cs sputter source and accelerated to 95 MeV using the FSU Tandem Van de Graaff Superconducting LINAC facility. The 20 mg/cm^2 natural Fe target (92% ^{56}Fe) stopped the beam and residual nuclei, but did not stop evaporation protons above 4 MeV. One Compton-suppressed Ge detector was used in coincidence with a 10-segment fast-slow plastic phoswich scintillator which covered most of the full sphere. For each coincidence event $E, \Delta E$, and timing information was digitized and written to tape for all segments along with the Ge energy signal. In the off-line analysis, two-dimensional gates were set for the proton region in each of the $E - \Delta E$ planes, and the γ spectrum was gated according to the number of protons detected in that event. Portions of the one- and two-proton spectra are shown in Fig. 2. Some of the strongest lines in the decay sequence above the isomer are seen clearly in the 1p spectrum, but not in the 2p spectrum. This proves that the decay sequence discussed below is associated with one proton evaporation from the ^{85}Zr compound nucleus and hence with a Y isotope. Although the charged particle evaporation information does not determine the neutron number, the excitation curve discussed above assigned a mass of 82 to the same decay sequence. Together these provide a firm assignment to ^{82}Y.

B. Prompt γ-γ coincidence measurements

An array of five BGO Compton-suppressed HPGe detectors was used in the γ-γ coincidence experiment. Two of these detectors were placed at 30° from the beam axis, and the rest at 90°. The ^{56}Fe(^{29}Si,$p2n$)^{82}Y at 95 MeV was also used in this experiment. The beam was provided by the FSU Tandem-Superconducting LINAC facility, and a 78 mg/cm^2 natural Fe (92% ^{56}Fe) target was used. At this energy, production of ^{82}Y represented about 10% of the 10^8 twofold coincidences written to tape.

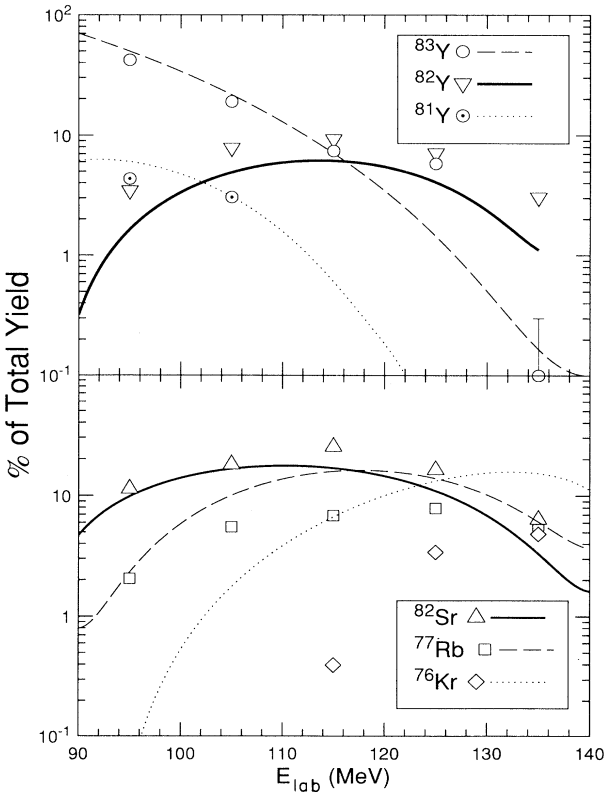

FIG. 1. Experimental and theoretical percentages of total yield versus beam energy (lab) for the bombardment of ^{28}Si ions on a ^{58}Ni target. Lines (points) represent the predicted (measured) percent of total yield. Error bars on the experimental points are smaller than the symbol size.

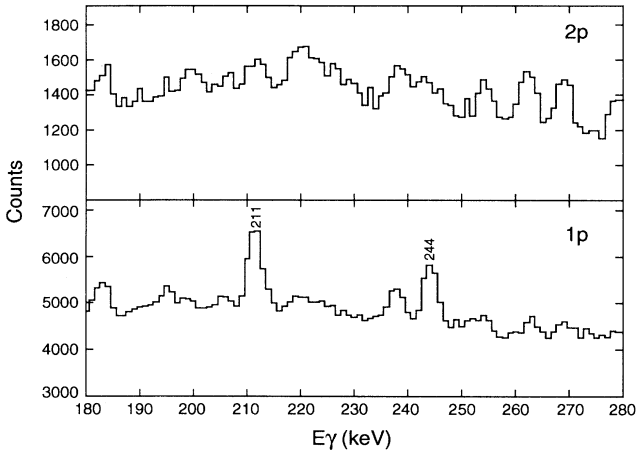

FIG. 2. A portion of the γ spectra in coincidence with one or two protons detected in the full-sphere phoswich detector.

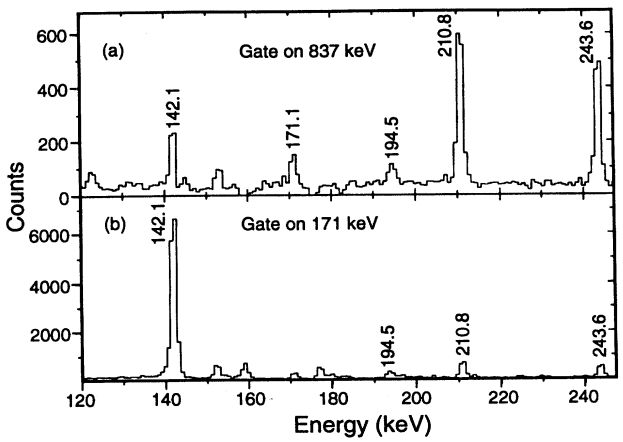

FIG. 4. Portions of the γ spectra in coincidence with the 171 and 837 keV transitions.

The data were sorted off-line into two arrays : a 90°-90° triangular array, and a 30°-90° square array with a dispersion 0.8 keV/channel. To better resolve low energy multiplets, coincidences from all the detectors were also sorted into a 0.5 keV/channel triangular array. Coincidences in the 30°-90° array were used to deduce lifetimes via the Doppler-shift attenuation method (see Sec. IV A.), and to determine directional correlation of oriented states (DCO) ratios.

The existence of a long-lived isomer (over 30 ns) for the 507 keV level (see Fig. 3) was inferred from this coinci-

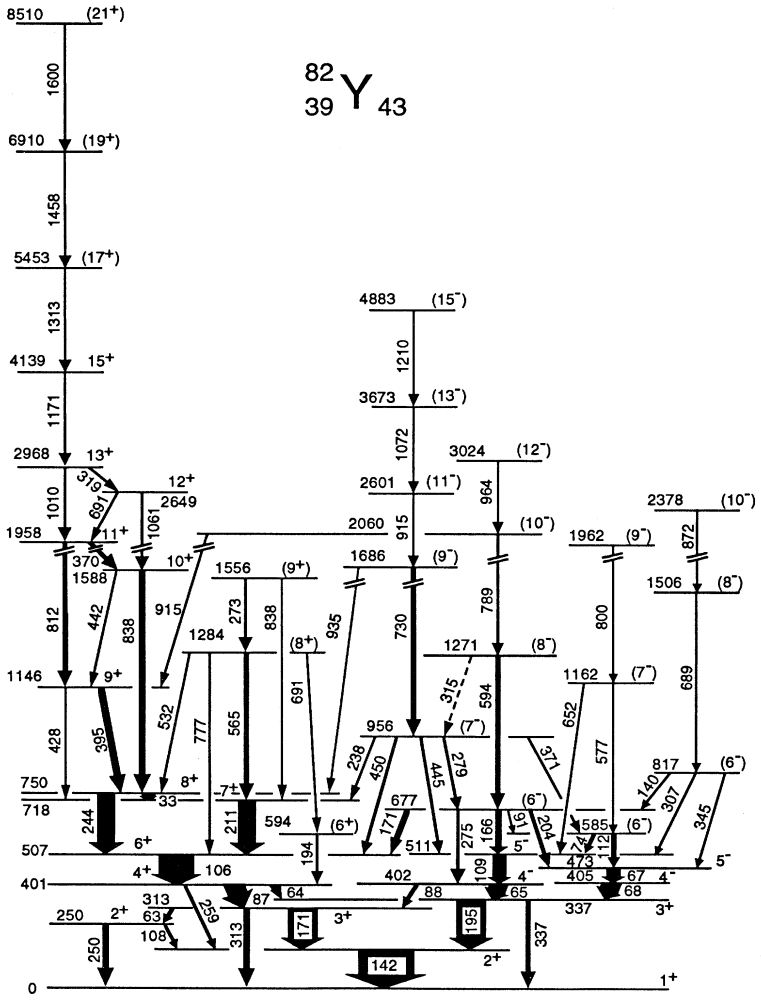

FIG. 3. The level scheme of ^{82}Y as deduced from the present work. The spin and parity assignments are discussed in the text.

TABLE I. Energies, branching ratios (R_B), DCO ratios, and multipolarities for transitions in ^{82}Y.

E_{LEV} (keV)	I_i^π	I_f^π	E_γ (keV)	R_B (%)	R_{DCO}
142.1	2^+	1^+	142.1(2)	100	
250.0	2^+	1^+	250.1(1)	75(2)	
		2^+	107.7(3)	25(2)	
313.4	3^+	1^+	313.5(3)	29.2(8)	
		2^+	63.4(3)	28.8(8)	
		2^+	171.1(2)	42.0(14)	
336.8	3^+	1^+	336.9(1)	37.0(5)	
		2^+	194.5(1)	63.0(5)	
400.7	4^+	3^+	87.2(2)	65.3(9)	
		3^+	64.0(2)	29.1(9)	
		2^+	258.7(1)	5.4(5)	
401.8	4^-	3^+	65.0(3)	33.2(9)	
		3^+	88.5(2)	66.8(9)	
405.0	4^-	3^+	68.2(3)	100	
472.5	5^-	4^-	67.5(3)	100	
506.7	6^+	4^+	106.0(3)	100	
510.8	5^-	4^-	109.0(1)	100	
585.0	(6^-)	5^-	112.4(2)	30(5)	
		5^-	74.2(2)	69(5)	
594.4	(6^+)	4^+	193.7(1)	100	
676.9	(6^-)	5^-	166.2(2)	26(3)	
		6^+	170.7(2)	32(4)	
		5^-	204.1(1)	20(3)	
		(6^-)	91.1(1)	2.5(3)	
		4^-	275.4(1)	18(3)	
717.5	7^+	6^+	210.8(1)	100	0.62(3)
750.3	8^+	6^+	243.6(1)	65(2)[a]	1.1(1)
		7^+	32.8[b]	35(2)[a]	
817.1	(6^-)	(6^-)	140.0(2)	28(6)	
		5^-	306.6(2)	22(7)	
		5^-	344.5(3)	49(9)	
955.8	(7^-)	7^+	238.1(2)	7.5(9)	
		(6^-)	279.0(2)	13(2)	
		(6^-)	370.3(2)	15.6(13)	
		5^-	445.1(1)	47(3)	
		6^+	449.6(2)	16.0(13)	
1145.5	9^+	8^+	395.2(2)	97.0(5)	0.4(1)
		7^+	428.0(2)	3.0(5)	
1162.1	(7^-)	5^-	651.5(2)	50(10)	
		(6^-)	576.8(2)	50(10)	
1271.0	(8^-)	(6^-)	593.9(3)	91.8(6)	0.94(8)
		(7^-)	315.3(2)	8.2(6)	
1283.5	(8^+)	8^+	532.3(2)	14.2(11)	
		7^+	565.2(2)	41(1)	
		(6^+)	690.8(4)	3.8(11)	
		6^+	776.7(3)	40(2)	
1505.6	(8^-)	(6^-)	688.5(3)	100	
1556.2	(9^+)	(8^+)	273.1(2)	11(7)	
		7^+	838.2(5)	88(7)	
1588.0	10^+	9^+	442.4(3)	12.9(8)	0.5(2)
		8^+	837.7(4)	87.1(8)	1.0(1)
1686.1	(9^-)	(7^-)	730.3(3)	85.1(6)	1.0(2)
		8^+	936.2(3)	14.9(6)	
1957.8	11^+	10^+	369.9(2)	51.6(8)	0.4(2)
		9^+	812.1(5)	48.4(8)	0.9(1)
1962.4	(9^-)	(7^-)	800.3(3)	100	
2059.9	(10^-)	(8^-)	788.7(4)	85(2)	0.98(9)
		9^+	914.5(3)	14(2)	
2377.9	(10^-)	(8^-)	872.3(4)	100	
2600.7	(11^-)	(9^-)	914.6(4)	100	

TABLE I. *(Continued).*

E_{LEV} (keV)	I_i^π	I_f^π	E_γ (keV)	R_B (%)	R_{DCO}
2649.0	12^+	10^+	1061.0(4)	82.7(8)	1.2(1)
		11^+	691.1(9)	17.3(8)	0.4(1)
2968.3	13^+	12^+	319.4(4)	26.1(8)	0.6(1)
		11^+	1010.4(5)	73.9(8)	1.2(1)
3023.5	(12^-)	(10^-)	963.6(9)	100	
3672.7	(13^-)	(11^-)	1072.0(9)	100	1.3(4)
4139.4	15^+	13^+	1171.1(7)	100	0.84(8)
4882.8	(15^-)	(13^-)	1210.1(9)	100	
5452.5	(17^+)	15^+	1313.1(5)	100	
6910	(19^+)	(17^+)	1458(1)	100	
8510	(21^+)	(19^+)	1600(1)	100	

[a]Branching ratio inferred from intensity balance.
[b]Energy inferred from level energies.

dence data. The intensity of the 142 keV ground state transition changes dramatically for all gates taken above and below the 507 keV level. For gates above, the 244 keV and 211 keV transitions are strongest [see Fig. 4(a)], and for gates below 507 keV of excitation, the intensity of the 142 keV line is greatly enhanced [see Fig. 4(b)]. These changes in relative intensity are characteristic of an isomer pushing some fraction of the transition intensity outside the 100 ns time window for prompt coincidences.

Gates on suspected $E2$ transitions were employed to measure the DCO ratios for states above the 507 keV isomer. The $E2$ nature of the gating transitions was verified by examining the DCO ratios of those transitions in other likely $E2$ gates. The results are tabulated in Table I together with γ-ray energies and branching ratios. A loss of alignment appears to occur at the 507 keV level due to its long mean lifetime, since the DCO ratios below it are all close to unity.

C. Delayed coincidence measurements

Because of the evidence for nanosecond isomers discussed above, two delayed coincidence measurements were performed using the ^{29}Si + ^{56}Fe reaction. In the first experiment, a time-to-amplitude converter (TAC) was started by a low energy photon spectrometer (LEPS) and stopped with either of two 75 mm x 75 mm NaI(Tl) detectors. Energies from the LEPS and time differences in a 1 μs range from the TAC were written to tape and subsequently sorted into a 2500×512 channel array. This data was used to determine the ns lifetimes. In the second experiment, a Compton-suppressed coaxial HPGe detector replaced the two NaI(Tl) detectors and HPGe-LEPS-TAC coincidences were recorded on 8 mm tape and sorted off-line. The statistics in the second experiment were not adequate to deduce further timing information, but prompt and delayed γ-γ coincidence matrices constructed from the data did provide an independent verification of the low-lying part of the level scheme aided by the higher energy resolution of the LEPS detector.

The TAC dispersion was measured by use of the 20.618 ns beam bursts of the FSU Superconducting LINAC. These beam bursts provided an excellent calibration of the system since the frequency of the rf signal of the LINAC system is known to a very high degree of precision. The beam bursts themselves appeared as small microstructure in the random coincidences of the TAC spectrum. They were particularly clear in a gate on the 847 keV $2^+ \rightarrow 0^+$ transition in ^{56}Fe which is very strong in singles and appears in the coincidence arrays mostly because of random coincidences. The beam burst structure appears only in the random coincidences and had little effect on the true coincidences. To prove that this microstructure came from the LINAC, a radioactive source test was performed in which this structure did not

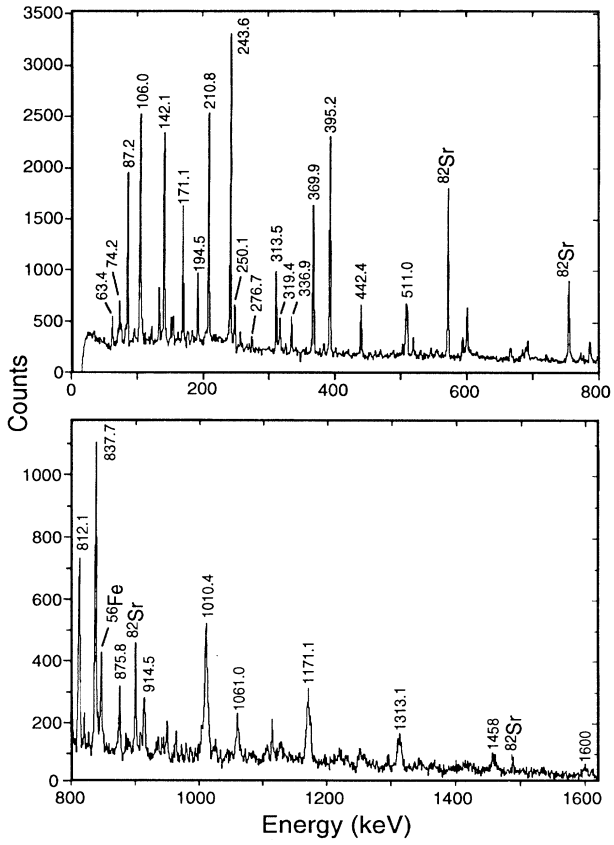

FIG. 5. The sum of γ spectra in coincidence with a number of transitions in the positive-parity band.

appear. In addition, this dispersion agreed within uncertainties with that measured by inserting a known delay into the stop signal. A discussion of lifetimes obtained by this method is given in Sec. IV B.

III. LEVEL SCHEME AND PROPERTIES OF ^{82}Y

A. Level scheme of ^{82}Y

No excited states were known in ^{82}Y from β-decay studies. We have assumed that the most intense γ ray at 142 keV decays directly to the 1^+ ground state. The low excitation region was not expected to exhibit the simplifying structure of rotational bands, and the existence of close-lying multiplets such as the five transitions between 63.4 and 68.2 keV also complicated the construction of the level scheme. On the basis of prompt and delayed coincidences, the level and decay scheme shown in Fig. 3 was constructed.

The most intense γ decay sequence passes through the 106 keV transition. A sum coincidence spectrum of decays in this sequence is shown in Fig. 5. The differences in coincidence strength above and below this isomer (Fig. 4) helped to place the decays in the level scheme. A transition between the closely spaced 750 and 718 keV levels could not be seen in any gate, but was inferred from the strong coincidences between the 395 and 211 keV lines. A 33 keV γ ray would have not have been visible in the Compton-suppressed Ge detectors because it was below the energy threshold and the probability for internal conversion is expected to be greater than for γ decay. Above 750 keV of excitation energy, the yrast band of the level scheme takes on the appearance of a good rotor and could be observed up to an energy of 8510 keV.

The strongest line in the second major decay sequence is at 109 keV ($5^- \rightarrow 4^-$). A loss of coincidence intensity above and below this transition indicates the existence of another isomer. As will be shown in Sec. IV B, the long-lived state is the 401.9 keV 4^- level into which the 109 keV transition feeds. The states in the 109 keV decay sequence are much weaker in intensity than those in the 106 keV sequence. Some transition energies in the 109 keV sequence are very close to others in the main decay sequence, such as the 370.3 keV ($7^- \rightarrow 6^-$) and the 369.9 keV ($11^+ \rightarrow 10^+$) transitions. Fortunately, coincidence spectra for these two are quite dissimilar, thus ruling out the possibility of the γ rays being the same. When the gates are not dissimilar, such as in the case of the 838.2 keV ($9^+ \rightarrow 8^+$) transition and the 837.7 keV ($10^+ \rightarrow 8^+$) transition, then intensity arguments were used to discern between these energies. A regular rotation-like level sequence appears above the 677 keV state and was observed up to a level at 4883 keV. Spin assignments for these states are discussed in the following subsection.

A third decay sequence involves the 68.2 and 67.5 keV transitions which are in cascade. Gates on the 204 and 279 keV γ rays show a prominent line at 68 keV. Upon closer inspection, a gate on the low energy part of this 68 keV line gives a peak near 68 keV but slightly higher in energy. A gate on the high energy part of the 68 keV line also returns a peak near 68 keV but somewhat lower in energy.

The level scheme of ^{82}Y contains four ns isomers: three lie at very similar energies of 401, 402, and 405 keV and the other directly above the 401 keV level at 507 keV. The lifetime measurements are discussed in Sec. IV B. Fortunately, these isomers are not long lived enough to cause a complete break in the coincidence data.

The preliminary report [11] of another investigation of ^{82}Y using the NORDBALL detector system shows a level scheme in good agreement with the present one. The only difference is the placement of the 7^+ level, whose position in the present level scheme is well fixed by connecting transitions. The NORDBALL experiment appears to have emphasized the high-spin structure and their level scheme extends to higher spins for the four bands reported, but low-spin states are not shown.

B. Spin assignments for ^{82}Y

Spin assignments can be made with reasonable certainty for most of the states in ^{82}Y. First the spin and parity of the ground state (gs) have been firmly established as 1^+ by two independent observations [7, 9] of allowed ^{82}Y β decay branches to both the 0^+ and 2^+ states of ^{82}Sr. Decay patterns and measured lifetime values or limits helped to determine the spins and parities of low-lying states, but the loss of alignment due to long-lived isomers precluded the use of angular distribution and correlation techniques for these states. Moreover, systematic comparisons with nearby odd-odd nuclei provided additional evidence about their spins and parities.

Above the low-lying states, several rotational bands appear. The one most strongly populated, which can be observed to the highest levels, is clearly the yrast band. The highest intrinsic spin available by far comes from the unique parity $g_{9/2}$ orbital, so that the yrast band at medium spins in odd-odd $A \approx 80$ nuclei is always based on a $(\nu g_{9/2} \otimes \pi g_{9/2})$ configuration. This fact and the great similarity between this band and positive-parity bands in other odd-odd nuclei (see Sec. V A) strongly suggests positive parity for the yrast band in ^{82}Y. A detailed comparison shows that rotation-like level spacing begins with the 8^+ state. This and the DCO value for the 244 keV transition establishes $I^\pi = 6^+$ for the 507 keV state.

The following discussion shows that the 6^+ assignment to the 507 keV state is consistent with the ground state spin and observed decay patterns and lifetimes. The measured long lifetime [$\tau = 212(10)$ ns] for the 507 keV level would imply for the 106 keV decay a reasonable $E2$ strength of 6.8(3) Weisskopf units (W.u.), but an unacceptably large $M2$ strength of 334(16) W.u. While a possible $M1$ strength of 1.1×10^{-4} W.u. or $E1$ strength of 2×10^{-6} W.u. cannot be completely ruled out, they are very unlikely because other decay paths would then be available.

The reasoning above gives an assignment of 4^+ to the 400.7 keV level, which itself has a mean lifetime of 16(4) ns (see Sec. IV). This lifetime is too short for any decay multipolarity higher than 1 for its low energy 64.0 and 87.2 keV decay branches. $E1$ decay for these branches is ruled out because it would lead to spin-parity assignments of 3^- to the 337 or 313 keV states and subsequent $M2$ decays to the 1^+ gs. The lifetimes of the 313 and

337 keV states must be less than 10 ns or they would have been observed in the timing experiment, so the g.s. $M2$ transition strengths would have unacceptably large values greater than 20 W.u. The 259 keV transition is consistent with a weak $E2$ strength of 0.09 W.u., but not an unacceptably high $M2$ strength of 5.4 W.u. A spin change of $1\hbar$ is ruled out for this transition since the subsequent 142 keV decay would have to carry away $2\hbar$ of angular momentum, leading to a long lifetime which was not observed. These arguments establish 3^+ for the 313 and 337 keV states and 2^+ for the 142 keV level. It should be remarked that all the decay branches of the 4^+ state are weak, with $M1$ strengths of about 0.002 W.u. and an $E2$ strength of 0.09 W.u. These low values are probably due to a major change of structure.

For the 250 keV level, both $M1$ and $E2$ decay modes to the g.s. are consistent with its lifetime limits. However, in the latter case the assignment would be 3^+, and the lifetime of the 400.7 keV level would be shorter, since a decay from this state to the 250 keV state would be allowed (about 150 keV). However, no such γ ray has been seen, and, if one were to exist, its transition probability would make it the most favored decay path. Since there is no evidence for this γ ray, we assign a spin and parity of 2^+ to the 250 keV state.

The transition probabilities for the 65.0 keV and the 88.5 keV transitions rule out anything but $E1$ or $M1$ decay. However, the $M1$ possibility would imply positive parity for the 401.8 keV state and allow a decay branch from the 507 keV state comparable in strength to that of the 106 keV transition. In the delayed coincidence TAC spectra of the 65.0 and 88.5 keV γ rays, there is nothing to suggest delayed feeding from a long-lived state. There is also no γ ray of such energy in either the 65.0 or 88.5 keV gates, nor is there any evidence for the 65.0 and 88.5 keV lines in the 106.0 keV gate. Hence, $I^\pi = 4^-$ for the 401.8 keV level. Similar arguments can be applied to the 405 keV level, leading also to a 4^- assignment.

Spin assignments for the states in the γ-decay sequence above the 6^+ isomer are based on the measured DCO ratios listed in Table I. Because DCO ratios could not be determined for transitions below the (7^-) state in the 109 keV decay sequence, their spin assignments are shown in parentheses. The spins shown are determined by systematics, but DCO ratios do establish the spin changes above the (7^-) state.

The tentative spin assignments given for the positive-parity bands in the NORDBALL level scheme of ^{82}Y [11] agree with the present assignments. No spins or parities were indicated in that level scheme for their bands "3" and "4" which correspond to the lowest negative-parity signature partner pair in the present level scheme.

IV. LIFETIMES OF STATES IN ^{82}Y

A. Lifetimes determined via Doppler shift attenuation method (DSAM)

DSAM lifetimes of the higher spin states were determined from a lineshape analysis of the measured peak shapes in the forward spectrum. In this analysis a computer code [13] was used which simulates the decay in flight process and generates a theoretical line shape for each lifetime using scaled stopping powers from Northcliffe and Schilling [14]. The lifetime value for the theoretical line shape which most closely reproduces the experimental one is the value taken for the lifetime of the state. The uncertainty in this procedure is determined by the rate of variation in the accuracy of the fit. The lifetimes of the highest measurable state for each cascade were extracted first, followed by the lower states. The direct feeding times for each state were specified by the lifetimes measured in the states above each. The highest measurable positive-parity state was the 19^+ state decaying by a 1458 keV transition, which was fitted to determine an effective lifetime for feeding corrections of the states below. Side-feeding times are more difficult to determine. We have employed the most commonly used procedure [13] of a short side-feeding time for the highest measurable state (0.03 ps) with an increase of about 0.04 ps for every MeV of deexcitation. Some researchers, see Ref. [15], have used longer side-feeding times, which would have led to shorter lifetimes and larger transition quadrupole moments. Examples of best fits are in Fig. 6. Values for lifetimes are tabulated in Table II.

B. Lifetimes via delayed coincidences

For this measurement, a time-energy array was created from the LEPS-NaI data. Gates were made on the γ ray of interest and the corresponding TAC spectra were analyzed. For decays with a single long lifetime, the TAC spectrum was converted to a semilogarithmic graph, and thus the lifetime could be determined by a simple least-

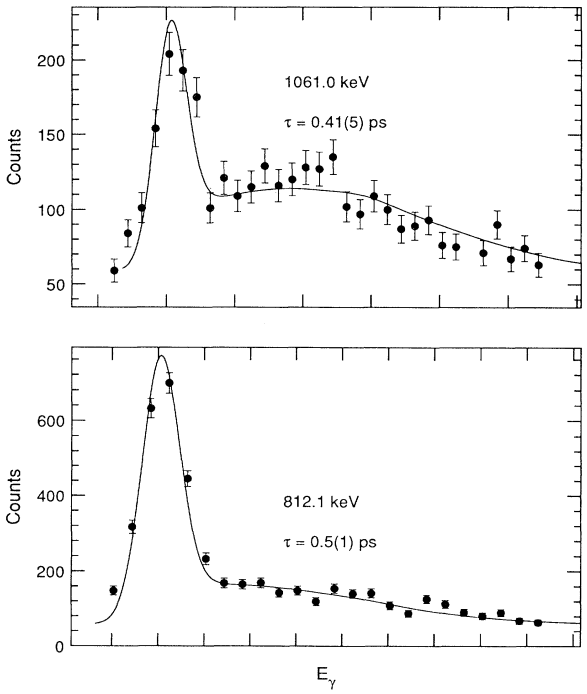

FIG. 6. Examples of forward-angle coincidence line shapes and the best-fit Doppler shift attenuation simulations.

TABLE II. Mean lifetimes in ^{82}Y measured by direct timing and by the Doppler-shift attenuation method, along with transition strengths $B(M1)$ or $B(E2)$ and transition quadrupole moments Q_t.

I_i^π	E_{LEV} (keV)	E_γ (keV)	τ_{exp}^{a} (ps)	τ_{acc} (ps)	$B(E2)$ (W.u.) [b]	Q_t (e b)
4^+	400.7	87.2	15(4)[c]	16(4)[c]	0.0015^{+4}_{-4} [d]	
		64.0	17(4)[c]		0.0017^{+5}_{-5} [d]	
		258.7			0.087^{+3}_{-3}	
4^-	401.8	65.0	373(47)[c]	387(36)[c]		
		88.5	400(24)[c]			
4^-	405.0	68.2	51(3)[c]	51(3)[c]		
6^+	506.7	106.0	212(10)[c]	212(10)[c]	6.8^{+3}_{-3}	
11^+	1957.8	812.1	0.5(1)	0.60(15)	88^{+30}_{-18}	$2.7\ ^{+4}_{-3}$
		369.9	0.8(2)			
12^+	2649.0	1061.0	0.41(5)	0.41(5)	58^{+8}_{-6}	$2.2\ ^{+1}_{-1}$
13^+	2968.3	1010.4	0.34(4)	0.34(4)	80^{+11}_{-8}	$2.5\ ^{+2}_{-1}$
15^+	4139.4	1171.1	0.19(2)	0.19(2)	92^{+11}_{-9}	$2.5\ ^{+2}_{-1}$
17^+	5452.5	1313.1	0.12(2)	0.12(2)	82^{+16}_{-12}	$2.4\ ^{+2}_{-2}$
(19^+)	6910	1458	<0.3	<0.3	> 20	>1.1
(11^-)	2600.7	914.6	0.45(7)	0.45(7)	$134\ ^{+25}_{-18}$	$3.4\ ^{+3}_{-2}$
(13^-)	3672.7	1072.0	0.24(3)	0.24(3)	$114\ ^{+16}_{-13}$	$2.9\ ^{+2}_{-2}$
(15^-)	4882.8	1210.1	<0.38	<0.38	> 40	>1.7

[a] Measured using the Doppler-shift attenuation method, unless indicated otherwise.
[b] 1 W.u. = 21.2 e^2 fm^4.
[c] In units of ns, measured by direct timing.
[d] $B(M1)$ in W.u.

squares fit to the slope. For a more complex decay such as the mother-daughter decay of the 400.7 keV state, a theoretical line shape was formed by fitting the formula

$$A_2(t) = N_0 \frac{\lambda_1\lambda_2}{(\lambda_1 - \lambda_2)} (e^{-\lambda_1 t} - e^{-\lambda_2 t}) \quad (1)$$

for the activity or decay rate of level 2, $A_2(t)$, to the TAC spectrum. Since Eq. (1) (which assumes no other feeding path to level 2) is symmetric with respect to the decay constants λ_1 and λ_2 for levels 1 and 2, it was fortunate that a gate could be made on the 106 keV transition to obtain its lifetime and decay constant λ_1. The values of λ_2 were then varied to best fit the experimental decay curve for the 400.7 keV level. To check for systematic error, the lifetime of the 6^+ state in ^{82}Rb, whose decay transition also appears in the data array was remeasured to be 20 ± 2 ns, which agrees well with the published value of 20 ± 3 ns [16]. Examples of the fits are shown in Fig. 7 and the lifetimes determined are tabulated in Table II.

Lifetimes of 150 and 260 ns are indicated for the 507 and 402 keV states in the NORDBALL level scheme of ^{82}Y [11]. If these represent half-lives, then the corresponding mean lifetimes of 216 and 375 ns would be in good agreement with the values determined in the present work.

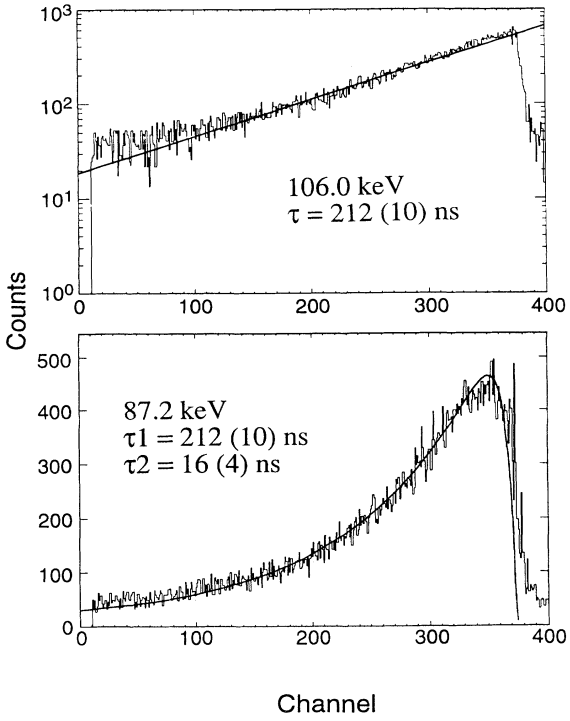

FIG. 7. Examples of the time spectra in coincidence with the 106.0 (top) and 87.2 keV (bottom) transitions. Note that time increases toward the left and a logarithmic scale was used for the ordinate in the top graph. The curves represent a single lifetime of 212 ns on top and a cascade of 212 and 16 ns on the bottom.

V. DISCUSSION

A. ^{82}Y in relation to neighboring nuclei

A direct comparison of the yrast bands of ^{82}Y, ^{80}Rb [3], and ^{84}Nb[17] is shown in Fig. 8. Since all the spins for ^{84}Nb in Ref. [17] are shown relative to unknown band-

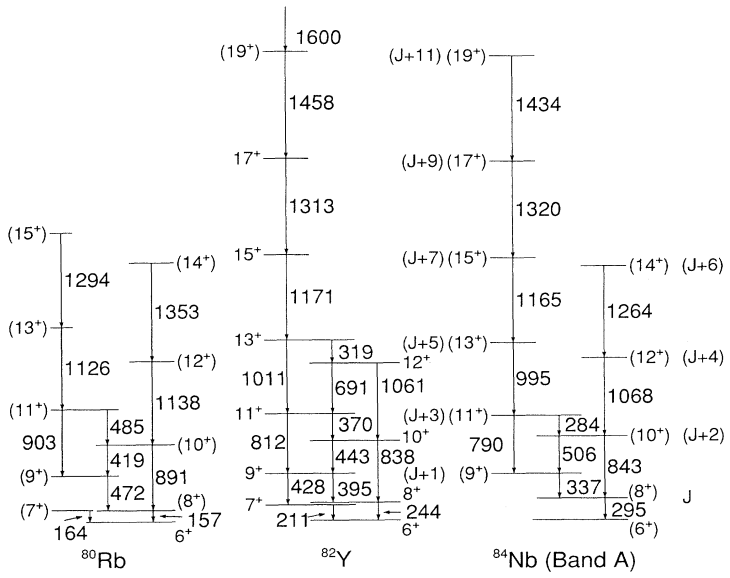

FIG. 8. Comparison of the level schemes for the yrast bands of the odd-odd $N = 43$ isotones. Spins and parities have been tentatively assigned to ^{84}Nb as discussed in the text.

head values, we have proposed tentative spins and parities on the basis of systematics. First, band "A" in the ^{84}Nb level scheme is proposed to be yrast because it was observed to the highest spins. Like all other yrast bands in odd-odd $A \approx 80$ nuclei it would then have positive parity. In Fig. 8, both ^{80}Rb and ^{82}Y have $8^+ \rightarrow 6^+$ transition energies less than 300 keV and $10^+ \rightarrow 8^+$ transition energies of about 850 keV. If one examines ^{84}Nb, the transition between J and the unnamed state has an energy below 300 keV, and the energy of the $J+2 \rightarrow J$ transition is about 850 keV. These correspondences strongly suggest that J is $8\hbar$, the value adopted for this comparative analysis. Note that the 631 keV transition shown in band A of the level scheme of Ref. [17] as a dashed line would be a very unlikely $\Delta I = 3$ decay under these assumptions and has been omitted from Fig. 8.

As can be seen from Fig. 8, the positive-parity band in ^{82}Y is rather similar to those of its neighboring odd-odd isotones. The transition energies are close to those in ^{84}Nb and a little smaller than those in ^{80}Rb. The signature splitting seems to increase somewhat with increasing Z. The 7^+ state is nearly degenerate with the 8^+ level and lies slightly higher in ^{80}Rb and slightly lower in ^{82}Y and has not been observed in ^{84}Nb.

Band "B" in the ^{84}Nb level scheme [17] most likely has negative parity. There is an ambiguity of $1\hbar$ in comparing its spins with those of its neighbors. For the analysis, we have chosen a value of $K = 5$ which gives the same phase of signature splitting as in the adjacent odd-odd isotones (see Sec. V B). Note that the spins of all the $\pi = -$ states being compared have some degree of uncertainty.

B. Cranking model analysis

The rotational bands in ^{82}Y have been analyzed in the framework of the cranking model [18], along with the nearby $N = 43$ isotones ^{80}Rb and ^{84}Nb and $Z = 39$ isotopes (^{81}Y [19] and ^{83}Y [20]).

The kinematic moments of inertia $J^{(1)}$ for the yrast band in ^{82}Y are compared with those of neighboring isotones (isotopes) in the top (bottom) part of Fig. 9. The behavior of $J^{(1)}$ for the three isotones is quite similar, as might be expected from Fig. 8. The values are some-

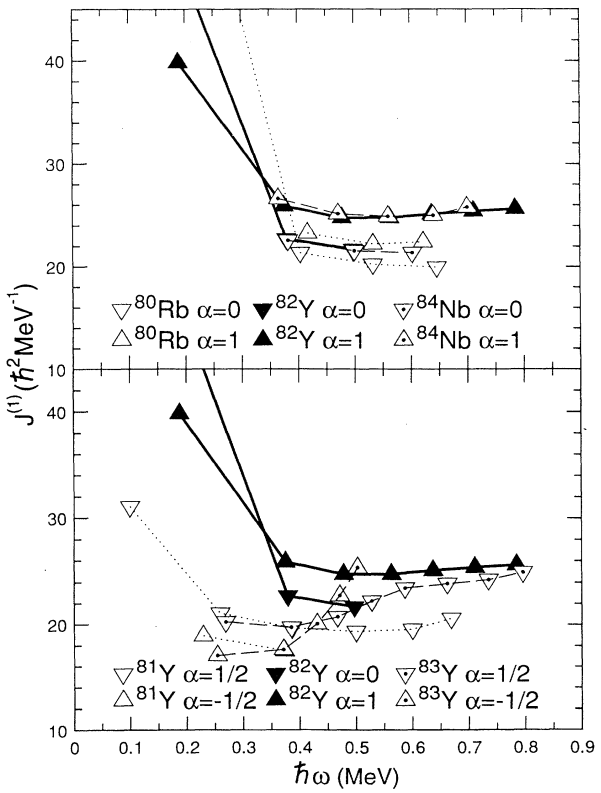

FIG. 9. The kinematic moments of inertia $J^{(1)}$ for the yrast bands of ^{82}Y and neighboring nuclei. The odd-odd $N = 43$ isotones, ^{80}Rb, ^{82}Y, and ^{84}Nb, are compared in the top part of the figure and the $Z = 39$ isotopes ^{81,82,83}Y in the bottom. The lowest frequency point for both ^{80}Rb and ^{82}Y is off-scale.

times rather high at low frequencies, but become quite constant above 0.4 MeV/$\hbar$ where they lie in the range of 20 to 25 $\hbar^2$/MeV—approximately the rigid rotor value. A similar behavior can be seen in the neighboring odd A isotopes whose moments of inertia also tend to saturate in the 20 to 25 $\hbar^2$/MeV range in agreement with a recent survey [21]. One difference is an alignment in the yrast band of ^{83}Y at $\hbar\omega \approx 0.45$ MeV which is presumably blocked by the odd neutron in ^{82}Y.

The experimental Routhians for ^{82}Y and its neighboring isotones are compared in Fig. 10 for both the lowest positive- and negative-parity bands. The Harris parameterization for the core reference energy ($J_0 = 14\ \hbar^2$/MeV and $J_1 = 6\ \hbar^4$/MeV^3) was taken from that used previously for ^{75}Kr [22]. The signature splitting clearly increases with increasing Z in the bands of both parities, and a signature inversion occurs at the lowest frequency in the positive-parity band.

Another quantity which shows the degree of signature splitting without a Harris parametrization is $(E_I - E_{I-1})/2I$. This expression is graphed as a function of I in Fig. 11 for the $N = 43$ isotones, ^{78}Br [23], ^{80}Rb, ^{82}Y, and ^{84}Nb. For a perfect rotor with no signature splitting, this quantity has a constant value of $\hbar^2/2\theta$, while signature splitting gives rise to an alternating pattern. All of these curves exhibit signature splitting with a magnitude generally increasing with increasing Z, as described above. A careful examination of the positive-parity graphs shows that the phase of the alternations reverses between 9$\hbar$ and 10$\hbar$ for ^{82}Y and between 10$\hbar$ and 11$\hbar$ for ^{80}Rb. Such an inversion in the signature splitting has also been seen in ^{74}Br [1], ^{76}Br [2], and ^{84}Y [24]. Calculations using a 2-qp plus-rotor model [4] have attributed the inversion to a change from excitation modes involving both qp alignment and collective rotation at low spins to rotation only at high spins. The change is predicted to occur at 9$\hbar$, the maximum spin available from two different $g_{9/2}$ qp, in the non-interacting approximation. Interactions between the two qp may be responsible for the small shift observed in the inversion point.

The alternations in the three negative-parity bands shown in Fig. 11 have the same phase above 7$\hbar$, but opposite to that of the positive-parity bands. That is, the odd spin states are lower in energy or favored in the positive-parity bands, as expected theoretically, but the even spin states are favored in the negative-parity bands. However, one should remember that the spin assignments are less firm in the negative-parity bands of ^{80}Rb and ^{82}Y and those of ^{84}Nb were determined on the basis of consistency with the other two. There may be a phase change between 7$\hbar$ and 8$\hbar$ in ^{80}Rb, but only the 5$\hbar$ point is anomalous in ^{82}Y and regular alternations continue to the lowest observed spin in ^{84}Nb.

In conclusion, the cranking model analysis shows a consistent pattern among the odd-odd $N = 43$ isotones in both the lowest positive- and negative-parity bands. In signature splitting and other properties ^{82}Y lies between ^{80}Rb and ^{84}Nb.

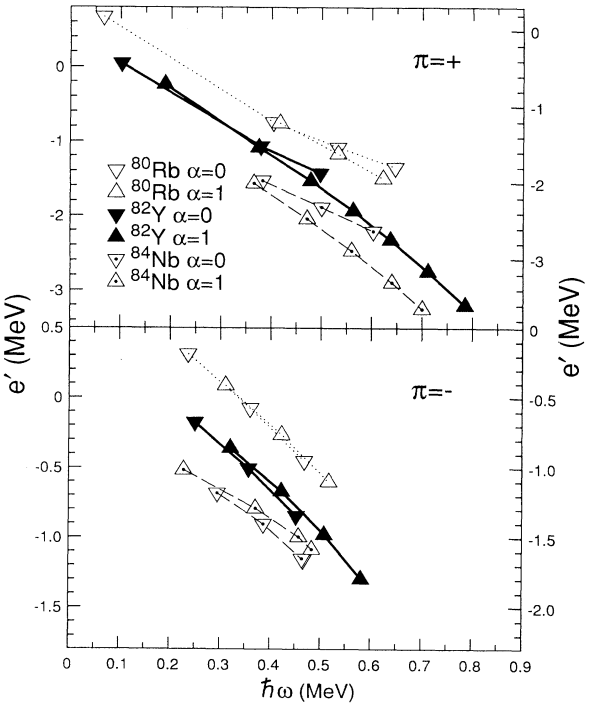

FIG. 10. Experimental Routhians for the odd-odd $N = 43$ isotones ^{80}Rb, ^{82}Y, and ^{84}Nb for the positive (top) and negative (bottom) parity bands. In both graphs the ordinate scale on the right applies to ^{80}Rb and the scale on the left to the other two nuclei. The Harris parameters used are $J_0 = 14$ $\hbar^2$/MeV and $J_1 = 6\ \hbar^4$/MeV^3.

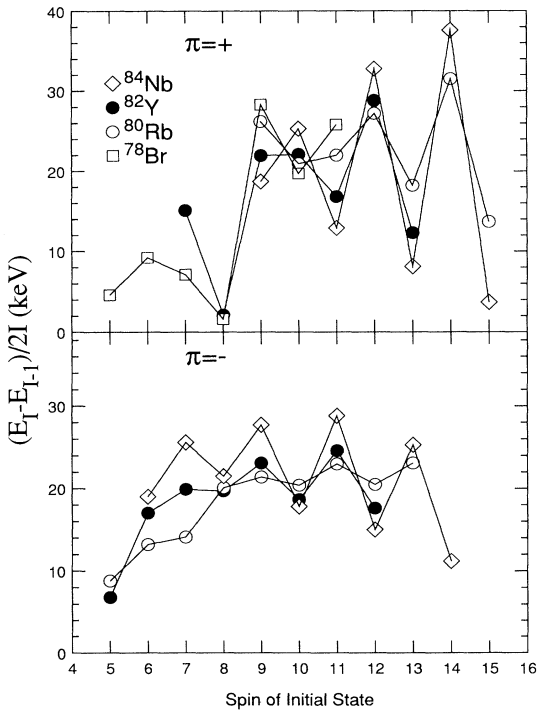

FIG. 11. Graph of the quantity $(E_I - E_{I-1})/2I$ as a function of I for the odd-odd $N = 43$ isotones ^{78}Br, ^{80}Rb, ^{82}Y and ^{84}Nb for the positive (top) and negative (bottom) parity bands. Data are available only for the positive-parity band of ^{78}Br.

C. Transition strengths and moments

The adopted lifetimes given in Table II were used to determine the electric quadrupole transition strengths $B(E2)$. These values, which are also listed in Table II, show a considerable collective enhancement of 50 to 120 W.u. The transition quadrupole moments Q_t were inferred from the $B(E2)$ values using the rotational model and are included in Table II.

Magnetic dipole transition strengths are sensitive to such parameters as triaxiality, signature splitting, and qp alignment. A number of $\Delta I = 1$ decays are seen in the yrast band, and their $M1$ values are displayed in Fig. 12 in two ways. The $B(M1)/B(E2)$ ratios inferred from the $\Delta I = 1$ to $\Delta I = 2$ branching ratios are shown on top. These values are based on a quadrupole-dipole mixing ratio of zero, which is approximately the value obtained from the DCO ratio of the $11^+ \rightarrow 10^+$ transition ($\delta = 0.02 \pm 0.20$). In any event the $B(M1)$ values vary with δ as $1/(1+\delta^2)$ and are rather insensitive to δ as long as it is small.

Since the $B(E2)$ values usually change slowly and smoothly in a rotational band (except near band crossings), the large alternations seen in the graph are most likely due to changes in the $M1$ strengths. This is confirmed by the behavior of the directly measured $M1$ strengths in the lower part of Fig. 12. The solid points based on lifetimes measured in the present work show large oscillations and reach values of more than 1 W.u. For completeness estimated $B(M1)$ values (assuming constant Q_t moments) are shown for the two lowest transitions whose lifetimes are too long to be measured by the DSAM.

Alternating $B(M1)$ values have recently been recognized in a number of $A \approx 80$ nuclei [25] in 1-qp or 2-qp bands. Among other odd-odd nuclei, they have been reported for ^{74}Br [1] and can be inferred from intensity tables in papers on ^{76}Br [2] and ^{78}Rb [26]. In 1-qp bands they have been observed in the $N = 41$ isotones ^{75}Se [5] and ^{77}Kr [27, 28] and interpreted in terms of triaxiality in the particle-rotor model [6]. There have also been two recent observations of alternating $M1$ strengths at high excitation in even-even ^{84}Sr [29] and ^{86}Zr [30], where the effect has been attributed to a doublet structure in the interacting boson approximation.

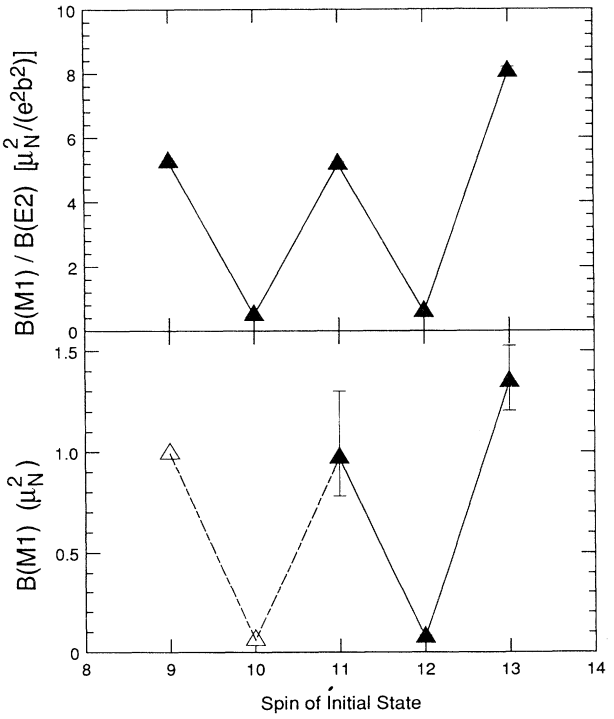

FIG. 12. Graphs of the $B(M1)$ strengths and $B(M1)/B(E2)$ ratios as a function of the spin of the initial state for the positive-parity band of ^{82}Y. Open symbols are used for the two points in the lower graph based on estimated, rather than measured, lifetimes. Error bars not shown for any closed symbol are smaller than the symbol size.

D. Hartree-Fock-Bogolyubov cranking calculations

The Woods-Saxon cranking model of Nazarewicz *et al.* [31] was used to calculate total Routhian surfaces for ^{82}Y. The rotation was treated by means of the cranking approximation with a monopole type of pairing force. More information about the calculation is given in Refs. [13] and [32].

In Fig. 13 there are four total Routhian surfaces [33] (TRS) in the (β_2, γ) plane. At each grid point, the Routhian was minimized with respect to the hexadecapole deformation β_4. For all four plots, the predicted β_2 deformation lies between 0.2 and 0.3 with γ between $-30°$ (triaxial) and $-52°$ (near oblate). The quasiparticle labeling scheme of Ref. [34] has been used. Lower (upper) case letters are used for the proton (neutron) configuration. For example the aA configuration shown in the top two graphs in Fig. 13 involves the lowest pos-

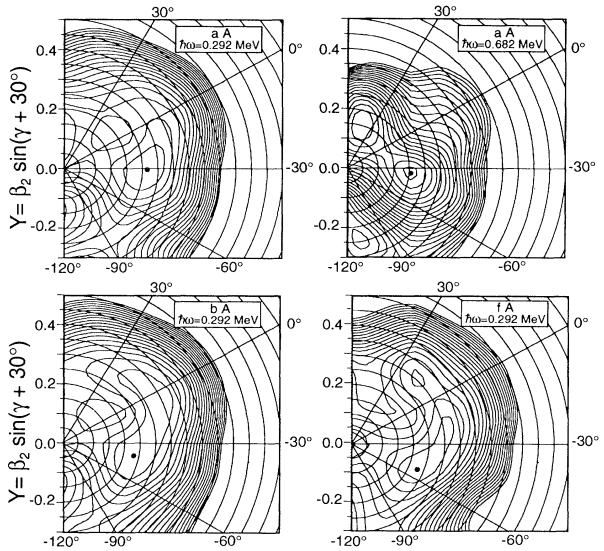

FIG. 13. Samples of total Routhian surfaces (with pairing) in the (β_2,γ) polar coordinate plane for ^{82}Y for two rotational frequencies. The frequencies and quasiparticle configurations are indicated in the inset boxes.

itive parity, signature $\alpha = +\frac{1}{2}$, proton and neutron orbitals for an overall positive parity and signature $\alpha = 1$. These plots are characteristic of the TRS for all frequencies in this configuration. The value of $\beta_2 \approx 0.23$ with $\gamma \approx -32°$ means that this is a triaxial nuclear shape with a moderate deformation. At $\hbar\omega = 0.682$ MeV, the TRS is somewhat γ soft with an additional local minimum at $\beta_2 = 0.15$ and $\gamma \approx 45°$. For the bA configuration which corresponds to positive parity with total signature $\alpha = 0$, we see a very similar TRS plot with a slightly more oblate shape ($\gamma \approx -40°$). This configuration seems also rather γ soft. Finally, the deformation for the fA configuration (the negative parity counterpart to the aA configuration) is similar to the other TRS but with a nearly oblate shape ($\gamma \approx -52°$).

The Q_t values calculated from the TRS deformations for these bands are rather similar, with an average value of about 2.5 e b. The predicted Q_t values vary little with frequency and generally agree well with the data, although both points for the negative-parity band are somewhat higher than the calculated ones.

E. Particle-rotor model calculations

In order to explore the observed behavior of the positive-parity band in greater detail, calculations have been made with the 2-qp plus triaxial rotor model described in Ref. [35]. In this approach, the 2-qp + rotor Hamiltonian is diagonalized numerically in a strong coupling basis built from selected proton and neutron Nilsson orbitals. The modified oscillator potential is used for the deformed mean field and the "standard" κ and μ parameters of Ref. [36] are adopted here, but with the proton parameters for $N = 3, 4$ used for both the protons and neutrons. This choice gives a very similar ordering and structure of Nilsson orbitals as the Woods-Saxon potential [31]. The positive-parity band is described in terms of positive-parity proton and neutron Nilsson orbitals, i.e., essentially the $\pi g_{9/2} \otimes \nu g_{9/2}$ configuration, although small components from other spherical orbitals are included. Calculations were made with the quadrupole deformation parameter $\epsilon = 0.23$ and a variety of γ values ranging from 0° (prolate shape) to 60° (oblate). These γ values correspond to the collective sector $-60° \leq \gamma \leq 0°$ in the TRS; however, note that a single core shape is used for all states in the particle-rotor model. The pairing gap and Fermi level are derived from the BCS treatment of pairing, and the core moments of inertia are calculated from the deformation parameters and the pairing gaps with the method of Ref. [37]. For example, at the prolate shape, this gave pairing gaps of 1.285 MeV (Δ_P) and 1.208 MeV (Δ_N) and a core 2^+ energy of 389 keV. No proton-neutron residual interaction was used. The intrinsic core $E2$ moments Q_0 and Q_2 were calculated microscopically, and the effective g_s factors for the odd proton and neutron were taken as 70% of the free values, and g_R was estimated as Z/A.

The calculated energy splitting $(E_I - E_{I-1})/2I$ is shown in Fig. 14(a), with different curves drawn for different values of γ. No attenuation of the Coriolis interaction is included. For the prolate shape, a pronounced staggering with the odd spins favored is present for $I \geq 10$ or so, and the phase of the staggering changes around $I = 9$, in rough agreement with the experimental data. This basic feature is found for all the shapes considered, even the oblate. The calculated neutron Fermi level is near the middle of the $g_{9/2}$ shell and is closest to the $\Omega = 5/2$ orbital for both the prolate and oblate shapes, while the proton Fermi level is below the $g_{9/2}$ shell and is closest to the $\Omega = 3/2$ orbital for the prolate shape and the $\Omega = 7/2$ orbital for the oblate shape. In all cases, the calculated wave functions are very mixed in the strong coupling basis, with the largest component about 15% (amplitude squared) for $I \approx 10$. Attenuating the Coriolis interaction (ξ) produces only modest improvement, as illustrated for the prolate shape in Fig. 14(b).

The $B(E2; I \rightarrow I-2)$ and $B(M1; I \rightarrow I-1)$ tran-

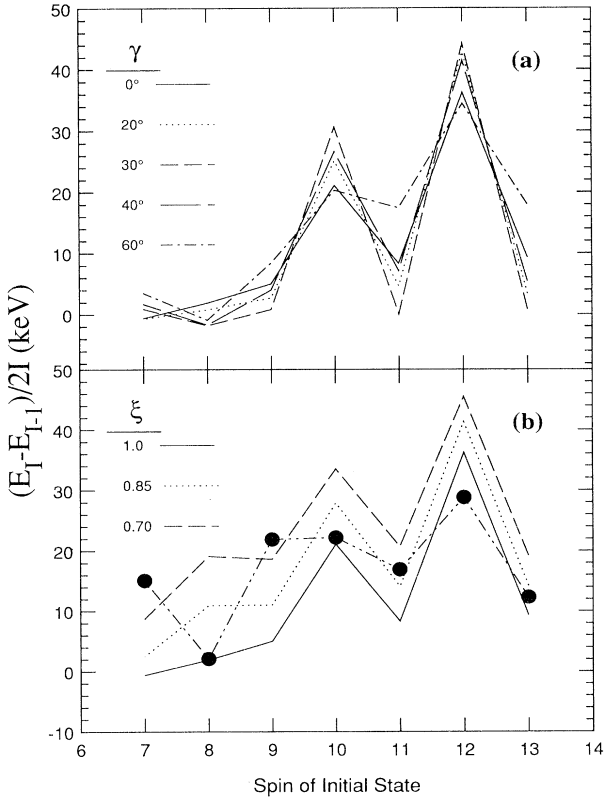

FIG. 14. Graphs of the quantity $(E_I - E_{I-1})/2I$ as a function of I calculated in the particle-rotor model. All the curves are calculated with a quadrupole deformation of $\epsilon = 0.23$. The top graph shows the dependence on the triaxiality parameter γ with no attenuation of the Coriolis term ($\xi = 1.0$). The bottom graph shows the effect of attenuating the Coriolis term by varying the parameter ξ in the case of prolate shape ($\gamma = 0°$). The experimental data points are shown on the bottom graph for comparison. The lines connecting the data points are drawn to guide the eye and do not represent any theoretical calculation.

sition strengths calculated for the different values of γ are shown in Fig. 15. These correspond to the states of Fig. 14(a). The general magnitude of the calculated $B(E2)$ values agrees rather well with the data for the prolate shape but not for the oblate, for which the intrinsic quadrupole moment is smaller in magnitude ($Q_0 = +2.33$ b and $Q_0 = -1.84$ b, respectively). Note that the observed staggering in the $B(E2)$ values is obtained for a "prolatish" triaxial shape, with $\gamma \approx 25°$. Also, the experimental $B(M1)$ strengths are well described in the calculations with either a prolate shape or "prolatish" shape, except for the point at $I = 13$. Again the oblate shape is clearly ruled out by the calculations, although the same phase of the staggering occurs for oblate as well as prolate shape. It is interesting to note that the contributions to the $M1$ transition rate from the odd proton and the odd neutron oscillate in phase for all these calculations, but that the odd neutron gives the larger contribution for the prolate case while the odd proton gives the larger contribution in the oblate case. The calculated $B(M1)$ values are very large (approximately $1.7\mu_N^2$) for $I = 8$ and $\gamma = 40°$ or $60°$ and are not shown on the graph. Finally, negative $E2/M1$ mixing ratios are obtained for all shapes considered here, so agreement with the data for this sign cannot be taken as conclusive evidence of a prolate shape as was proposed for ^{84}Y [24]. In particular, the calculated mixing ratio for the $11^+ \rightarrow 10^+$ transition is negative but small enough in magnitude that it agrees with the data within error bars for prolate, oblate, and triaxial shapes.

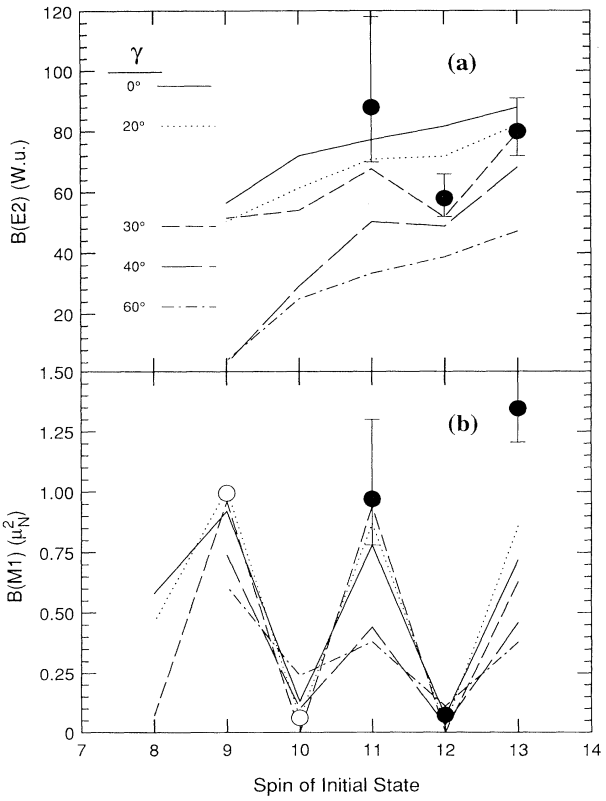

FIG. 15. Comparisons of (a) electric quadrupole and (b) magnetic dipole transition strengths calculated in the particle-rotor model with the measured quantities. The calculations display the variation with the triaxiality parameter γ, holding the magnitude of the deformation constant at $\epsilon = 0.23$ with no attenuation of the Coriolis coupling ($\xi = 1.0$).

Thus, qualitative agreement with the experimental positive-parity band is obtained for prolate or "prolatish" triaxial shapes. The observed energy splitting including the change of phase at low spins is qualitatively reproduced, while the strong staggering in the $B(M1)$ strengths is very well described. The observed staggering in the $B(E2)$ values suggests a triaxial core shape, with $\gamma \approx 25°$. These results agree qualitatively with the TRS calculations. Finally, preliminary calculations including a residual interaction do not seem to give any essential changes or improvements.

VI. SUMMARY

In-beam γ-ray techniques have been used to identify and study excited states in ^{82}Y. Transitions in ^{82}Y were identified by a comparison between the measured excitation curve and statistical model predictions and by detecting the evaporated charged particles in a segmented full-sphere phoswich scintillator. Prompt and delayed γ-γ coincidences were measured using the ^{56}Fe(^{29}Si,$p2n$)^{82}Y reaction. Positive- and negative-parity rotational bands were observed up to tentative spins and parities of (21^+) and (15^-). DCO ratios were used to determine the spins of high-lying states, while those of low-lying states were determined from transition probabilities and systematic considerations. The mean lifetimes of a number of states were determined using the Doppler-shift attenuation method, and the lifetimes of four ns isomers were measured by direct timing.

A positive-parity band has been identified in ^{82}Y which is very similar to those in the odd-odd $N = 43$ isotones ^{80}Rb and ^{84}Nb. A cranked shell model analysis revealed that the kinematic moments of inertia in this band become rather constant at approximately the rigid body value of (20 to 25)$\hbar^2$/MeV above a frequency of 0.4 MeV/$\hbar$, in agreement with the neighboring isotones. All three isotones show a similar signature splitting pattern whose magnitude increases with increasing Z. The energy splitting exhibits a phase inversion at about $10\hbar$ which has been attributed to a transition from particle realignment to collective rotation in other odd-odd nuclei. Another type of signature splitting was seen in the $B(M1)$ strengths which alternate in magnitude by a factor of 10.

A more weakly populated negative-parity band was also seen in ^{82}Y and is similar to those in the neighboring odd-odd isotones. The signature splitting in this band is opposite to that in the positive-parity band.

Hartree-Fock-Bogolyubov cranking calculations predict a moderately deformed ($\beta_2 \approx 0.25$) triaxial shape for the positive-parity band and an almost oblate shape of similar deformation for the negative-parity band. The

transition quadrupole moments Q_t implied by these shapes are close to those inferred from the measured lifetimes.

Two-quasiparticle plus rotor calculations for the positive-parity band indicate that the observed energy splittings and $B(M1)$ and $B(E2)$ strengths are consistent with a prolate or "prolatish" triaxial core shape.

ACKNOWLEDGMENTS

This work was supported in part by the National Science Foundation and in part by the U.S. Department of Energy under the grant DE-FG05-92ER40694 (P.B.S.). We are grateful to W. Nazarewicz for providing his Hartree-Fock-Bogolyubov cranking calculations for ^{82}Y.

[1] J.W. Holcomb, T.D. Johnson, P.C. Womble, P.D. Cottle, S.L. Tabor, F.E. Durham, and S.G. Buccino, Phys. Rev. C **43**, 470 (1991).

[2] S.G. Buccino, F.E. Durham, J.W. Holcomb, T.D. Johnson, P.D. Cottle, and S.L. Tabor, Phys. Rev. C **41**, 2056 (1990).

[3] J. Döring, G. Winter, L. Funke, B. Cederwall, F. Lidén, A. Johnson, A. Atac, J. Nyberg, G. Sletten, and M. Sugawara, Phys. Rev. C **46**, R2127 (1992).

[4] A.J. Kreiner and M.A.J. Mariscotti, Phys. Rev. Lett. **43**, 1150 (1979).

[5] T.D. Johnson, T. Glasmacher, J.W. Holcomb, P.C. Womble, S.L. Tabor, and W. Nazarewicz, Phys. Rev. C **46**, 516 (1992).

[6] G.B. Hagemann and I. Hamamoto, Phys. Rev. C **40**, 2862 (1989).

[7] C.J. Lister, P.E. Haustein, D.E. Alburger, and J.W. Olness, Phys. Rev. C **24**, 260 (1981).

[8] C. Deprun, S. Della Negra, J.P. Husson, H. Gaovin, and Y. Le Beyec, Z. Phys. A **295**, 103 (1980).

[9] S. Della Negra, H. Gauvin, D. Jacquet, and Y. Le Beyec, Z. Phys. A **307**, 305 (1982).

[10] C.J. Lister, private communication.

[11] J. Mukai, A. Odahara, R. Nakatani, H. Tomura, S. Suematsu, S. Mitarai, T. Kuroyanagi, D. Jerrestam, J. Nyberg, G. Sletten, A. Atac, S.E. Arnell, H. Roth, and Ö. Skeppstedt, in *Abstracts 21. INS International Symposium of Rapidly Rotating Nuclei, 1992* (University of Tokyo, Tokyo, 1992), p. 44.

[12] A. Gavron, Phys. Rev. C **21**, 230 (1980).

[13] E.F. Moore, P.D. Cottle, C.J. Gross, D.M. Headly, U.J. Hüttmeier, S.L. Tabor, and W. Nazarewicz, Phys. Rev. C **38**, 696 (1988).

[14] L.C. Northcliffe and R.F. Schilling. Nucl. Data Sec. A **7**, 233 (1970).

[15] F. Cristancho, K.P. Lieb, J. Heese, C.J. Gross, W. Fieber, Th. Osipowicz, S. Ulbig, K. Bharuth-Ram, S. Skoda, J. Eberth, A. Dewald, and P. von Brentano, Nucl. Phys. **A501**, 118 (1989).

[16] J. Döring, L. Funke, W. Wagner, and G. Winter, Z. Phys. A **339**, 425 (1991).

[17] C.J. Gross, K.P. Lieb, D. Rudolph, M.A. Bentley, W. Gelletly, H.G. Price, J. Simpson, D.J. Blumenthal, P.J. Ennis, C.J. Lister, Ch. Winter, J.L. Durell, B.J. Varley, Ö. Skeppstedt, and S. Rastikerdar, Nucl. Phys. **A535**, 203 (1991).

[18] R. Bengtsson, S. Frauendorf, and F.-R. May, At. Data Nucl. Data Tables **35**, 15 (1986).

[19] C.J. Lister, R. Moscrop, B.J. Varley, H.G. Price, E.K. Warburton, J.W. Olness, and J.A. Beckner, J. Phys. G **11**, 969 (1985).

[20] C.J. Lister, B.J. Varley, W. Fieber, J. Heese, K.P. Lieb, E.K. Warburton, and J.W. Olness, Z. Phys. A **329**, 413 (1988).

[21] S.L. Tabor, Phys. Rev. C **45**, 242 (1991).

[22] A.A. Chishti, W. Gelletly, C.J. Lister, J.H. McNeill, B.J. Varley, D.J.G. Love, and Ö. Skeppstedt, Nucl. Phys. **A501**, 568 (1989).

[23] M. Behar, D. Abriola, A. Filevich, G. García-Bermúdez, A.J. Kreiner, M.A.J. Mariscotti, A.A. Pinston, and D. Barneoud, Nucl. Phys. **A376**, 131 (1982).

[24] S. Chattopadhyay, H.C. Jain, J.A. Sheikh, Y.K. Agarwal, and M.L. Jhingan, Phys. Rev. C **47**, R1 (1993).

[25] S.L. Tabor, T.D. Johnson, J.W. Holcomb, P.C. Womble, J. Döring, and W. Nazarewicz, in *Proceedings of the International Conference on Nuclear Structure at High Angular Momentum* (Atomic Energy of Canada, Chalk River, Ontario, 1992), Vol. 2, p. 322.

[26] G.C. Hicks, C.J. Gross, U.J. Hüttmeier, Xi-Ting Lu, G. Neuschaefer, and S.L. Tabor, Phys. Rev. C **30**, 549 (1984).

[27] T.D. Johnson, J.W. Holcomb, P.C. Womble, P.D. Cottle, S.L. Tabor, F.E. Durham, S.G. Buccino, and M. Matsuzaki, Phys. Rev. C **42**, 2418 (1990).

[28] C.J. Gross, P.D. Cottle, D.M. Headly, U.J. Hüttmeier, E.F. Moore, and S.L. Tabor, Phys. Rev. C **36**, 2601 (1987).

[29] P. Chowdhury, C.J. Lister, S.J. Freeman, D. Vretenar, A. Galindo-Uribarri, D. Radford, D. Ward, and V.P. Janzen, Bull. Am. Phys. Soc. **37**, 1279 (1992).

[30] P. Chowdhury, C.J. Lister, D. Vretenar, Ch. Winter, V.P. Janzen, H.R. Andrews, D.J. Blumenthal, B. Crowell, T. Drake, P.J. Ennis, A. Galindo-Uribarri, D. Horn, J.K. Johansson, A. Omar, S. Pilotte, D. Prévost, D. Radford, J.C. Waddington, and D. Ward, Phys. Rev. Lett. **67**, 2950 (1991).

[31] W. Nazarewicz, J. Dudek, R. Bengtsson, T. Bengtsson, and I. Ragnarsson, Nucl. Phys. **A435**, 397 (1985).

[32] U.J. Hüttmeier, C.J. Gross, D.M. Headly, E.F. Moore, S.L. Tabor, T.M. Cormier, P.M. Swertka, and W. Nazarewicz, Phys. Rev. C **37**, 118 (1988).

[33] W. Nazarewicz, private communication.

[34] R. Wyss, F. Lidén, J. Nyberg, A. Johnson, D.J.G. Love, A.H. Nelson, D.W. Banes, J. Simpson, A. Kirwan, and R. Bengtsson, Nucl. Phys. **A503**, 244 (1989).

[35] I. Ragnarsson and P. B. Semmes, Hyp. Int. **43**, 425 (1988).

[36] T. Bengtsson and I. Ragnarsson, Nucl. Phys. **A436**, 14 (1985).

[37] R. Bengtsson and S. Åberg, Phys. Lett. B **172**, 277 (1986).